Low Dose of Amino-Modified Nanoparticles Induces Cell Cycle Arrest

Jong Ah Kim,[†,‡] Christoffer Åberg,[†,‡] Guillermo de Cárcer,[§] Marcos Malumbres,[§] Anna Salvati,[‡,*] and Kenneth A. Dawson[‡,*]

[‡]Centre for BioNano Interactions, School of Chemistry and Chemical Biology & UCD, Conway Institute for Biomolecular and Biomedical Research, University College Dublin, Belfield, Dublin 4, Ireland, and [§]Cell Division and Cancer Group, Spanish National Cancer Research Centre (CNIO), Madrid, Spain. [†]J.A.K. and C.Å. contributed equally to this work.

ABSTRACT The interaction of nanoscaled materials with biological systems is currently the focus of a fast-growing area of investigation. Though many nanoparticles interact with cells without acute toxic responses, amino-modified polystyrene nanoparticles are known to induce cell death. We have found that by lowering their dose, cell death remains low for several days while, interestingly, cell cycle progression is arrested. In this scenario, nanoparticle uptake, which we have recently shown to be affected by cell cycle progression, develops differently over time due to the absence of cell division. This suggests that the same nanoparticles can trigger different pathways depending on exposure conditions and the dose accumulated.

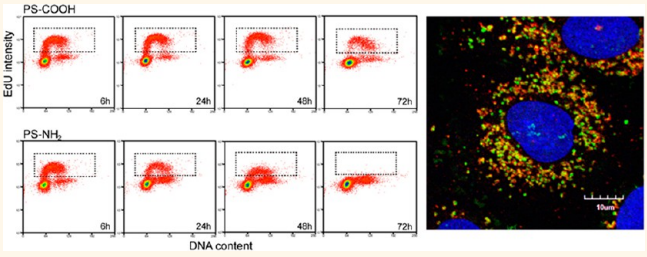

KEYWORDS: nanoparticle · cell cycle arrest · nanotoxicity · cationic nanoparticles · nanoparticle uptake · lysosome · cell division

Thanks to their unique attributes, nanoparticles can enter cells and interact with the cellular machinery using energy-dependent pathways.[1−3] For this reason, nanoparticle interactions with biological systems are being investigated for their potential in nanomedicine.[4−8] Although several nanoparticles accumulate in cells with no acute toxicity,[3,9] some nanomaterials have been found to impact cells and this has generated nanosafety concerns.[10−13] Cytotoxic responses have been associated to nanoparticles such as metal oxide ones and fullerenes,[14−18] where the effect can be connected mainly to the release of toxic ions due to particle solubility,[19] oxidative stress,[17,20,21] and cationic damage.[20] Recent studies have shown that alterations of the native structure of the proteins that adsorb on the nanoparticles' surface in the context of biological fluids can trigger signaling cascades and activate inflammatory responses.[22] Some positively charged polymeric nanoparticles such as the amino-modified polystyrene nanoparticles (PS-NH_2) used here, have previously been shown to induce cell death,[20,23,24] interfere with the cell cycle,[25] and more recently, to induce inflammation.[26] Upon their internalization by cells, PS-NH_2 nanoparticles accumulate in the lysosomes, like several other nanoparticles of different materials and sizes.[3,9,27,28] We have previously shown that nanoparticle accumulation is, in this case, accompanied by strong lysosomal swelling, followed by lysosomal membrane damage, which in turn leads to the leakage of proteolytic enzymes into the cytosol, triggering the apoptotic cascade.[20] Mitochondrial damage and production of reactive oxygen species have also been described for these nanoparticles.[20,23]

Here we report that by lowering the dose administered to lung epithelial A549 cells to a level where cell death is not predominant, PS-NH_2 can induce a form of cell cycle arrest. The cell cycle encompasses all the events during a cell's life that lead to its duplication and division, and its disruption and deregulation is at the origin of carcinogenesis and cell death.[29] However, induction of cell cycle arrest is often the basis of anticancer

* Address correspondence to kenneth.a.dawson@cbni.ucd.ie; anna.salvati@cbni.ucd.ie.

Received for review November 3, 2012 and accepted August 13, 2013.

Published online August 13, 2013
10.1021/nn403126e

therapeutics.[30] Interestingly, nanoparticles similar to the ones used here but with carboxylated surface modification (PS-COOH) do not show any cytotoxic effect over wide concentration ranges.[20] Here we show that, despite having the same final intracellular destination in the lysosomes,[3,31] low doses of amino-modified, but not carboxylate-modified, nanoparticles prevent cell proliferation and induce a series of toxic responses. They inhibit both DNA synthesis and cell division, although the metabolic status of the cells seems unaffected and energy-dependent processes such as nanoparticle uptake do not stop. In recent work we showed that the nanoparticle dose of a cell population decreases over time due to cell division and also described how this dilution can be distinguished from other phenomena, such as export of nanoparticles out of the cell.[31] Because PS-NH_2 impair cell division, we were able to observe how the absence of dilution of the intracellular load affects the uptake and accumulation dynamics of a population, and this allowed us to further confirm the intimate connection between nanoparticle accumulation and cell cycle progression.

Overall, these results suggest that a given nanoparticle is potentially able to activate very different pathways, depending on the exposure conditions and the dose achieved. This also opens up the possibility of discovering fundamental connections between cell death mechanisms and cell cycle pathways. Moreover, the induction of cell cycle arrest combined with the unique capacity of nanoscaled objects to cross biological barriers makes these materials, provided careful targeting, appealing for the development of novel therapeutic strategies.

RESULTS AND DISCUSSION

Lung cancer epithelial A549 cells were incubated with 25 μg/mL PS-NH_2 or PS-COOH nanoparticles for different exposure times. Time-resolved characterization of the nanoparticle dispersions (Supporting Information, Figure 1 and Table S1) showed that the nanoparticle size in cell culture medium increased compared to the stocks in water, but overall the dispersions remained stable for the full duration of the experiment, showing no signs of agglomeration over time. It is known that in biological fluids nanoparticles can adsorb proteins and other biomolecules from the surrounding environment, forming a so-called biomolecular corona,[32−34] consistent with the increase in size in cell culture medium. A further consequence of this is that nanoparticles of opposite charge, such as the PS-COOH and PS-NH_2 nanoparticles used here, acquire a similar zeta potential, closer to neutrality due to screening of the surface charges.[24] It has been shown that the corona composition changes for particles of different surface charge.[35] Despite this, the two polystyrene nanoparticles used here appear to behave rather similarly when interacting with cells, both following the endolysosomal pathway after internalization for final accumulation in the lysosomes.[3,20,24,31] Once there, however, different outcomes are observed.

A cell viability ATP assay (Figure 1a) showed that for higher doses of PS-NH_2 nanoparticles strong cell death occurred, while no cell death was detected for cells exposed to the PS-COOH nanoparticles, consistent with literature.[23−26,31] However, for PS-NH_2 low levels of cell death were observed for concentrations lower than 100 μg/mL for these particular cells.[20] Moreover, monitoring of cell numbers revealed that at these lower doses cell proliferation took place during the first 24 h of treatment, but over longer incubation times cell numbers did not increase, in contrast to untreated cells in the same conditions (Figure 1b). Notably, cell numbers did not decrease during the treatment either, suggesting a rather delicate balance between cell division and cell death, or else an arrest of cell cycle progression (or some element of both of these processes).

In order to analyze cell cycle progression during exposure to the nanoparticles, a double staining technique was performed combining the nucleoside analogue EdU (5-ethynyl-2′-deoxyuridine) and the DNA dye 7-AAD (7-Aminoactinomycin D). All experiments (unless otherwise noted) were performed on asynchronous cell cultures, where cells are found distributed among all cell cycle phases. Prior to nanoparticle exposure, cells were labeled with EdU which only labels cells in the S phase of the cell cycle, since it is actively incorporated into the DNA during DNA synthesis. The dye 7-AAD was used to stain the total DNA of all the cells at the end of the nanoparticle incubation time. Figure 1c shows that as cell division takes place, the fluorescence due to EdU is diluted over time as the EdU-labeled DNA is distributed among daughter cells. This can be observed for untreated cells (top row) as well as for nanoparticle-treated ones (bottom row) although for the latter this was true only during the first 24 h of exposure. Incubation with PS-NH_2 nanoparticles for longer than 24 h resulted in rather unchanged EdU fluorescence levels, which suggests that less cell division took place during incubation with the nanoparticles. Together, the results in Figure 1b,c suggest that during the first 24 h of exposure to PS-NH_2 nanoparticles the cells were still able, at least in part, to undergo cell division, but were impaired to continue to do so for exposure times longer than 24 h. Thus, the PS-NH_2 nanoparticles were capable of interfering with cell cycle progression.

Given that DNA synthesis is a tightly regulated process that is sensitive to insults to cells[36,37] and that the nucleoside analogue EdU only labels cells that are actively synthesizing DNA, we also used the EdU/7-AAD staining *after* applying the nanoparticle treatment in order to estimate the percentage of

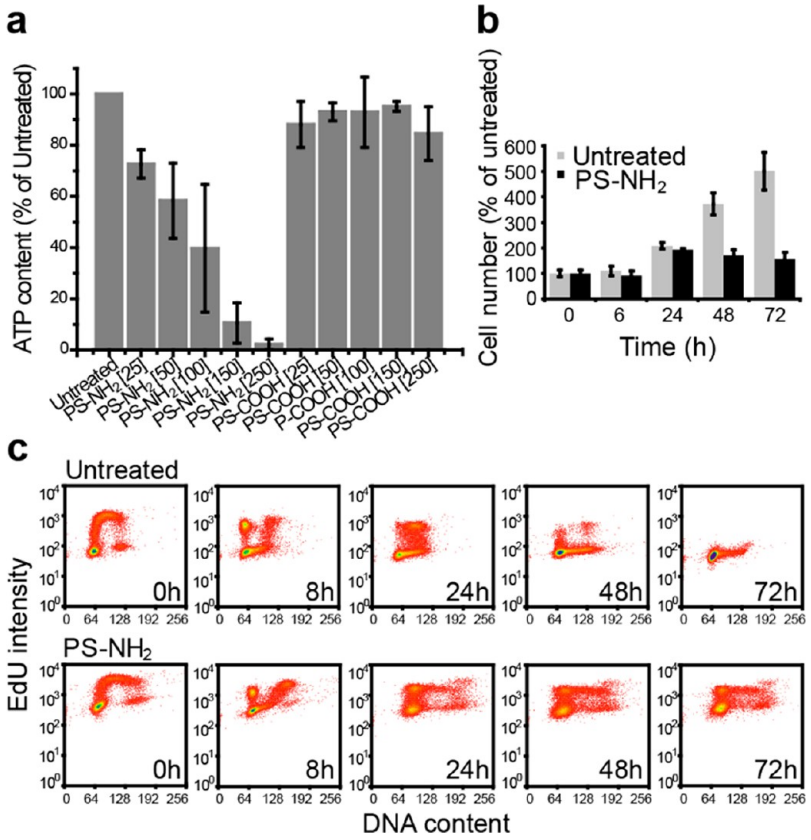

Figure 1. Low dose of amino-modified polystyrene nanoparticles inhibits cell proliferation. (a) ATP cell viability assay after 24 h of incubation with amino-modified (PS-NH_2) or carboxylated (PS-COOH) polystyrene nanoparticles at 25−250 μg/mL. Error bars represent standard deviation over three independent experiments. (b) Cell numbers of cultures incubated with cMEM or 25 μg/mL PS-NH_2 nanoparticles for 6−72 h, expressed as percentages of the number of untreated cells at the start of the experiment (0 h). (c) EdU-DNA scatter plots of cells labeled with EdU and incubated with cMEM (untreated, above) or 25 μg/mL PS-NH_2 nanoparticles (PS-NH_2, below) for 6−72 h, obtained by flow cytometry.

proliferative cells remaining after different exposure times (Figure 2a). The percentage of proliferative cells in the S phase decreased dramatically from 40% in untreated cells to 10% in PS-NH_2-treated cells after 24 h of incubation (Figure 2b). The proliferative fraction of cells continued to decrease until its total extinction after 72 h of PS-NH_2 treatment, indicating an increasing inhibition of DNA synthesis. In contrast, in the case of untreated cells, only after 48 h of incubation a small decrease in the level of EdU incorporation could be detected, which then became more evident after 72 h exposure, as is usually observed after sustained cell proliferation and nutrient depletion during such long incubation times. Importantly, PS-COOH-treated cells behaved similarly to untreated ones, suggesting that the carboxylated nanoparticles did not induce any cell cycle perturbation, which is in line with our previous work.[31] Given their lack of impact on the cell cycle these nanoparticles have been used here as a negative control and to illustrate the connection between the observed outcomes and different nanoparticle surface modifications.

To determine whether the described effect is solely observed in A549 cells, we performed similar experiments in a different cell line. The treatment with PS-NH_2 had a similar impact on a human colon carcinoma (HCT 116) cell line (Supporting Information, Figure 2a), which was found to have a similar nanoparticle uptake rate as A549 cells (Supporting Information, Figure 2b). We also assessed whether the effect of PS-NH_2 could depend on the tumor suppressor protein p53. p53 is a major regulatory protein which plays a pivotal role in controlling the fate of damaged cells that have the potential of becoming cancerous.[38] It inhibits their multiplication and stimulates their death in an attempt to block tumor development.[39] Importantly, we found that upon exposure to PS-NH_2, DNA synthesis was also inhibited in HCT cells that lacked a functional p53 protein, as shown by a comparable decrease of EdU-positive cells in p53-null and p53-wild type HCT cells. Overall this suggests that the effect of PS-NH_2 nanoparticles can be reproduced in other cell types and, more importantly, that the effect is p53-independent (Supporting Information, Figure 2).

It is interesting to note that although the treatment with PS-NH_2 interfered with cell cycle progression and inhibited DNA synthesis (as indicated by the decrease in EdU incorporation levels), the cells did not accumulate largely in one specific phase, even after 72 h of treatment with PS-NH_2 (Figure 2b). This is in contrast

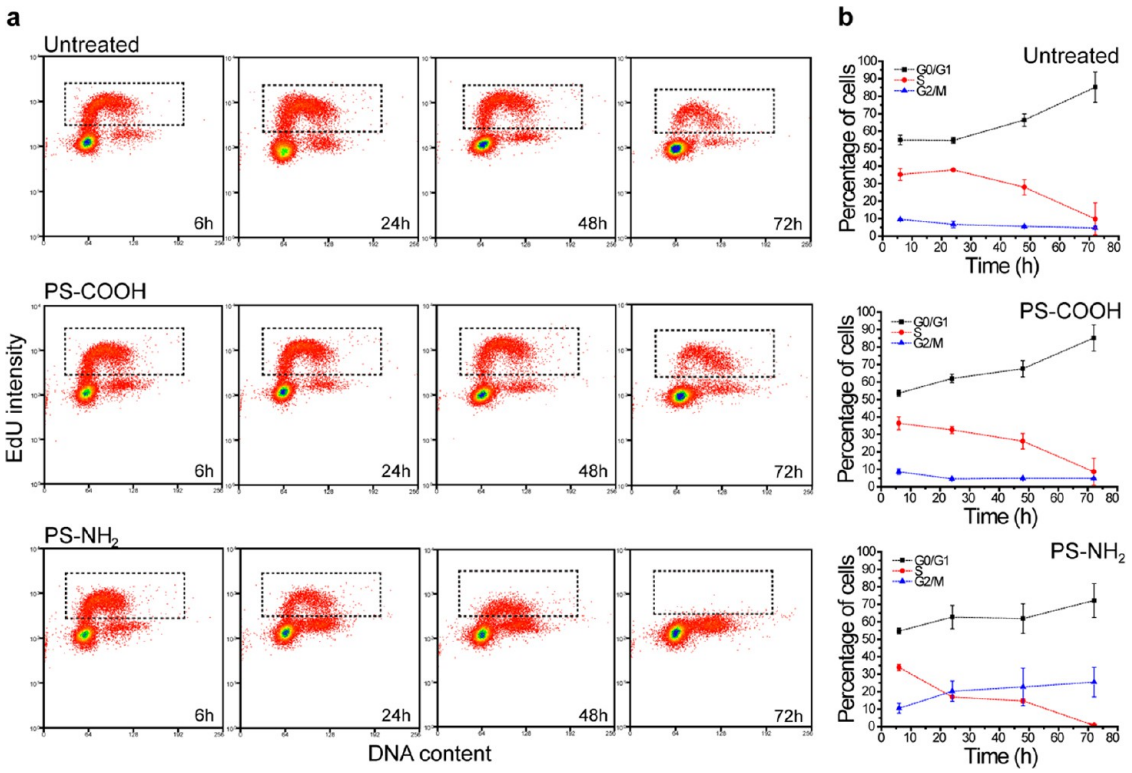

Figure 2. Amino-modified polystyrene nanoparticles induce cell cycle arrest and prevent DNA synthesis. (a) EdU-DNA scatter plots of cells incubated with EdU after their treatment with 25 μg/mL carboxylated (PS-COOH), amino-modified (PS-NH_2) polystyrene nanoparticles or nanoparticle-free medium (untreated) for 6−72 h. Dashed boxes indicate EdU-positive (S-phase) cells which were actively synthesizing DNA at each given time point. (b) Percentage of cells in the different cell cycle phases from the experiment shown in (a). Note that the percentage of proliferative (S-phase) cells decreases after 24 h of treatment with PS-NH_2 (whereas it decreases also for untreated cells and cells treated with PS-COOH, but only much later as a consequence of prolonged incubation times).

with what is usually observed after treatment with drugs that halt the cell cycle at a specific phase. For instance, treatment with paclitaxel causes cells to accumulate in mitosis and similarly aphidicolin causes a very strong increase in G1/S phase cell percentage.[40,41] A closer analysis of the subpopulations of cells in the different cell cycle phases (Figure 2b) revealed that while for untreated and PS-COOH-treated cells there was an increase in G1/G0 cells (as a consequence of confluence of the cell culture and lack of nutrients at long exposure times), PS-NH_2-treated cells exhibited a subtle increase in the percentage of cells in the G2/M phase and a corresponding decrease of those in the S phase. Such a scenario is consistent with a perturbation of cell cycle progression at multiple points along the cell cycle.

To support this interpretation, we performed numerical simulations of cell cycle progression with possible arrest at one or multiple points of the cell cycle, as illustrated in the schematic in Figure 3a (see Supporting Information for details of the simulations). In this endeavor, we built upon the quantitative agreement between our previous experimental characterization and theoretical modeling of the normal cell cycle progression of the same cell line.[31,42] We performed simulations for three possible scenarios: arrest at the G1/S boundary, the G2/M one, and arrest at both points (Figure 3a). Figure 3b shows the results in terms of the percentage of cells in the different phases after a time long enough for all cells to be arrested and no cell cycle progression to occur anymore. For arrest at the G1/S boundary (left) cells accumulate in G1, similar to aphidicolin treatment (see above). In contrast, arrest at the G2/M boundary (center) causes cells to accumulate in G2, as for paclitaxel treatment. We found that the experimental data, however, corresponds better to the third case (right), supporting the hypothesis of a block at multiple points of the cell cycle.

We also investigated the kinetics of cell cycle progression in the case of multiple arrest points with the simulations (Figure 3c). If each cell that reaches one of the two points is arrested at the moment it reaches the respective point, then all cells would be arrested within 10 h (left). If, on the other hand, cells that reach either point are only arrested 50% (center) or 25% (right) of the time, then arrest occurs more gradually. Naturally, there are complicating issues experimentally, such as the increase in the number of G1/G0 cells that occurs even for untreated cells at long incubation times (Figure 2b). Still, the slow changes in cell cycle phase populations that is observed experimentally for PS-NH_2-treated cells likely suggests a gradual arrest with time.

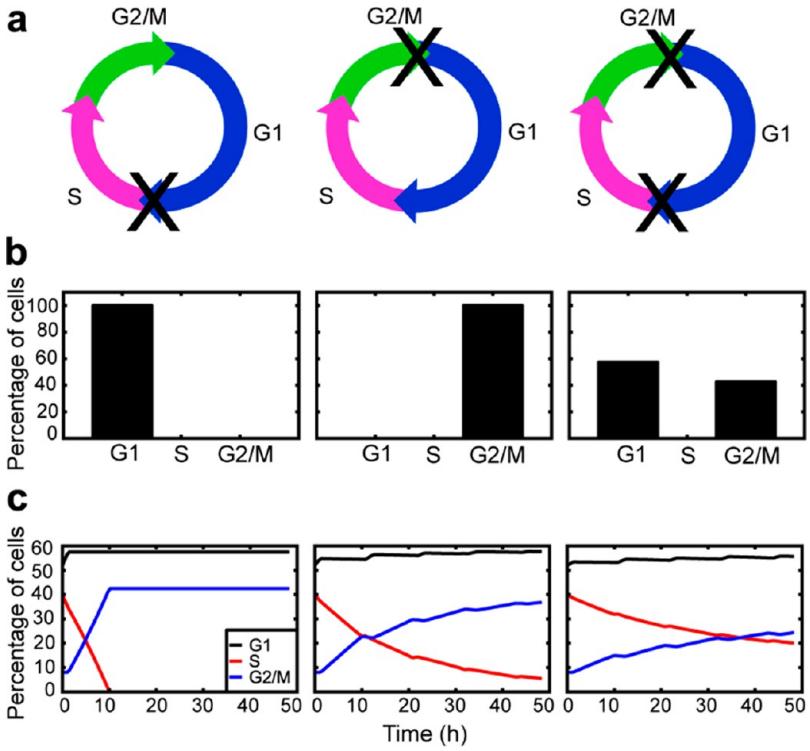

Figure 3. Amino-modified polystyrene nanoparticles arrest the cell cycle at two points and the arrest occurs gradually. (a) Schematics showing three possible arrest scenarios: progression blocked at G1/S boundary (left), G2/M boundary (center), or both (right). (b) Corresponding results of numerical simulations for the three scenarios, showing the cell cycle phases' distribution after the arrest has fully developed. (c) Numerical simulations of the kinetics of arrest assuming blockage at multiple points (right panels in a,b) and assuming all (left), 50% (center) or 25% (right) of cells reaching either point arresting.

Thus, the experimental observations (Figure 2) are consistent with an arrest that occurs gradually and that occurs at multiple points along the cell cycle. It is natural to identify the arrest points with the two cell cycle check points, and to better clarify this, further studies were performed. To experimentally analyze eventual effects on the G1/S checkpoint, we used a commonly applied method in which cells are synchronized in the M phase with nocodazole,[43] isolated as described in the Methods and subsequently seeded in the presence of medium (control), PS-COOH, or PS-NH_2 nanoparticles in order to monitor cell cycle progression through the G1/S checkpoint. The percentage of proliferating cells successfully entering in the S phase was measured by the incorporation of the nucleoside EdU (Supporting Information, Figure 3a). In the presence of PS-COOH nanoparticles, cells entered the S phase after 6−8 h, similarly to what is observed in the absence of nanoparticles. In contrast, in the presence of the PS-NH_2 nanoparticles only after 12−14 h some cells in S phase could be detected. This strongly suggests that the exposure to PS-NH_2 nanoparticles affects the G1/S checkpoint.

Similarly, to analyze the effect of PS-NH_2 treatment on the G2/M checkpoint, cells were synchronized in the G1/S transition with thymidine,[44] as described in the Methods, and then incubated with medium (control), PS-COOH, or PS-NH_2 nanoparticles. Progression of the cells into the M phase was indicated by staining with the MPM2 antibody, a mitotic marker[45] (Supporting Information, Figure 3b). The results indicated that cell cycle progression was not affected by exposure to PS-COOH nanoparticles, while exposure to PS-NH_2 delayed the entry into the M phase and/or made the cell population enter the phase in a more asynchronous fashion, as suggested by the belated and smaller increase of the percentage of MPM2-positive cells.

Although further experiments are needed in order to draw definite conclusions on this point, and, in general, about the arrest mechanism, a possible interpretation is that the treatment with PS-NH_2 primarily affected the G1/S checkpoint and that the alteration on G2/M progression was a secondary effect due to the interference at the G1/S boundary. Cancer cells like the cells used here are known to have aberrations that weaken their checkpoint mechanisms; thus, it is plausible that despite the nanoparticle-induced block at the G1/S checkpoint some cells would have anyway escaped and continued to cycle, but carrying with them a series of damages that would then perturb the G2/M progression later in their cell cycles.

To further characterize the observed arrest, we also monitored the levels of key regulators of the cell cycle. Cell cycle progression is tightly regulated by several protein families, among which cyclin proteins and their associated cyclin-dependent kinases (Cdk) play

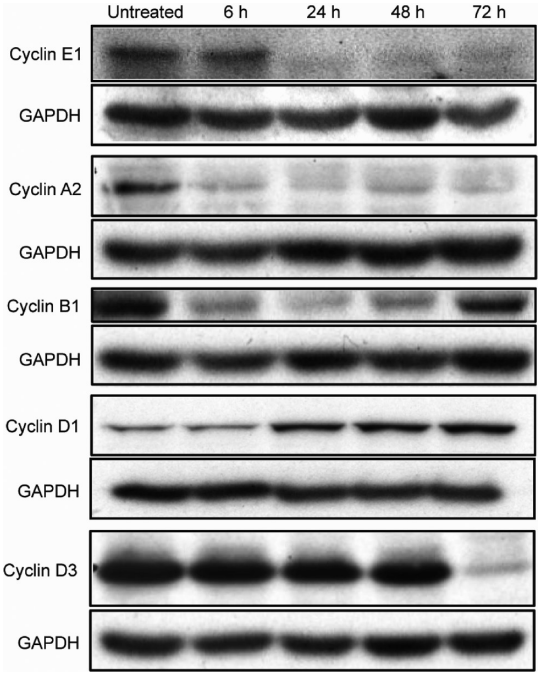

Figure 4. Western blot for cyclins E1, A2, B1, D1, and D3 of protein extracts of cells treated with 25 μg/mL amino-modified polystyrene nanoparticles for 6–72 h. GAPDH expression levels served as loading control.

a central role.[29] Figure 4 shows the analysis of the expression levels of some of the key cyclins (E1, A2, B1, D1, and D3) by immunoblotting. We observed several time-dependent changes in cells incubated with nanoparticles, compared to untreated cells. However, we focus the discussion on the onset of the arrest, as the interpretation of changes in cyclin levels at long incubation times is complicated by nutrition depletion and so on. A first important observation is that after only 6 h of exposure strong alterations of some of the cyclin levels were already observed. This indicates an earlier onset of the nanoparticle-induced effects than what could be detected with the EdU staining, which instead showed ongoing progression of the cell cycle at this exposure time (Figure 1c). In particular, the levels of cyclin E1 were drastically reduced after 24 h of exposure. E-type cyclins determine the passage to the S phase and their expression peaks between G1 and S phase,[46] where they bind to Cdk2 and promote the expression of cyclin A, which is in turn needed for the progression of the following S phase. The strong decrease of cyclin E1 and A2 supports the block at the G1/S checkpoint described above (Supporting Information, Figure 3). Cyclin A also binds to Cdk2 to promote S phase progression and a decrease in its levels is consistent with the reduction of EdU incorporation previously described (Figure 2). Similarly, cyclin B1, which peaks later on in the cell cycle at the G2/M checkpoint and forms a complex with Cdk1 that is largely responsible for commitment to cell division,[47] was observed to decrease already after 6 h, with a stronger effect after 24 h. Finally, after 24 h of treatment, the levels of cyclin D1 were affected as well. D-type cyclins drive progression into and across the G1 phase, binding to several Cdks, and, together with E-type cyclins, determine the entry into the S phase. Changes in cyclin D1 expression are consistent with the onset of the cell cycle arrest observed after 24 h in Figure 2. Interestingly, changes in cyclin D3 levels were instead observed only after 72 h of treatment when the level of cyclin B1 also seemed to be restored. However, as noted above while the analysis of cyclin levels gives insight on the onset of the observed arrest, the results at these late exposure times could be affected by complications such as nutrient depletion. (The cell cycle phase distributions and EdU incorporation results as shown in Figures 1 and 2, respectively, allow easier analysis of the effects observed at these longer exposure times.)

To further investigate the behavior and metabolic status of the arrested cells, we also measured the ATP content per cell after nanoparticle treatment. It should be noted that the experimental procedure in this case is (as detailed in the Methods) such that the ATP content is measured for the same number of cells in cultures treated with either PS-NH_2 or PS-COOH. The viability assay shown in Figure 1a is instead the average over all cells remaining after the treatments and is thus affected by cell numbers. We observed that the intracellular ATP content per cell (Supporting Information, Figure 4) decreased comparatively little after 24 h of exposure to nanoparticles, implying that the overall energy levels of the cells were largely unaffected by the treatment with PS-NH_2, despite the cell cycle arrest already being established.

We also monitored nanoparticle uptake and intracellular localization at the same exposure times. The time-resolved measurement of the cell fluorescence intensity by flow cytometry indicated continuous internalization of PS-NH_2 nanoparticles by the cells over the whole duration of the experiment (Figure 5a), even after the onset of cell cycle arrest. Interestingly, the uptake kinetics appears different from the uptake kinetics observed for PS-COOH nanoparticles (reproduced in Figure 5a from ref 31 to allow comparison). For PS-COOH, we have shown previously that the uptake kinetics was determined by a competition between nanoparticle uptake and cell division. In such a scenario, uptake kinetics show a linear increase during the first few hours, but after one day deviate from linearity due to dilution of the internalized nanoparticle load when cells divide. The competition between uptake and cell division eventually results in a plateau of the uptake kinetics, although other factors such as the cell culture reaching confluence and lack of nutrients most likely also play a role for late times.[31] In the case of the PS-NH_2 nanoparticles, the uptake kinetics appeared to follow the same trend of the PS-COOH nanoparticles during

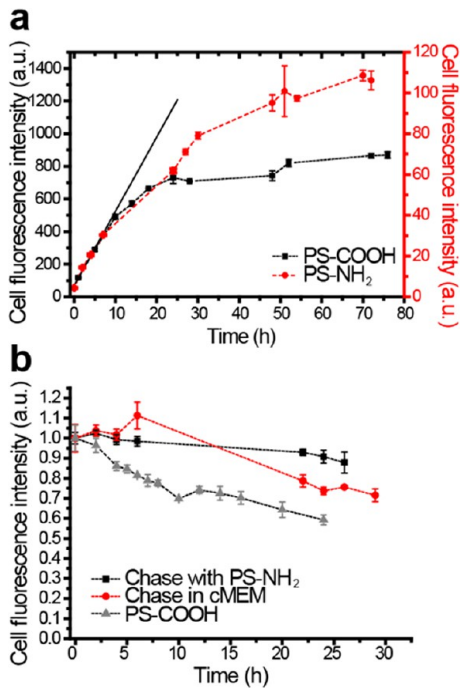

Figure 5. Effect of amino-modified polystyrene nanoparticle-induced cell cycle arrest on the uptake and accumulation kinetics of nanoparticles. (a) Cell fluorescence intensity due to continuous exposure to 25 μg/mL amino-modified (PS-NH_2; red) or carboxylated (PS-COOH; black) polystyrene nanoparticles as a function of time, measured by flow cytometry. Error bars represent standard deviation over three replicas. (b) Fluorescence intensity of cells exposed to 25 μg/mL PS-NH_2 for 24 h (thus, inducing cell cycle arrest) and further grown in nanoparticle-free medium (red) or medium containing nonfluorescent PS-NH_2 (black). The equivalent experiment for PS-COOH is shown for comparison (gray). Fluorescence values shown are normalized to the cell fluorescence measured after 24 h exposure (0 h from particle removal). In both panels, data for PS-COOH are reproduced from ref 31 and are included for comparison.

the linear regime for early times (a linear fit of the data for the first hours is also shown in Figure 5a to facilitate the observation). However, somewhat later a deviation from nonlinearity could be observed due to cell division for both treatments, consistent with some cell cycle activity still occurring in the cells treated with PS-NH_2 for these exposure times, as discussed above. However, after roughly 24 h of incubation, the uptake kinetics of PS-NH_2 nanoparticles continued to increase, whereas that of the PS-COOH ones started plateauing. This is certainly consistent with the PS-NH_2 inhibiting cell division, thus providing a means to avoid the competition between nanoparticle uptake and dilution due to cell division in favor of uptake. For later times (48 h and longer), there are necessarily complicating factors (for both types of nanoparticles) such as lack of nutrients, likely dominating the nonlinear behavior for PS-NH_2 uptake kinetics and also contributing to the plateau observed with PS-COOH at these late times. From a broader perspective, these results further confirm that nanoparticle accumulation is strongly connected to cell cycle progression, both for cases where no changes in cell cycle progression are induced (PS-COOH) as well as for cases where cell cycle progression is impaired (PS-NH_2).

Furthermore, by labeling S-phase cells with EdU and monitoring their fluorescence intensity during continuous exposure to fluorescent PS-NH_2, we could confirm experimentally that in the first hours of exposure to the nanoparticles, during which the cell cycle arrest is not yet established, the internalized dose of nanoparticles is diluted by cell division (as indicated by the lower fluorescence of cells that have just divided compared to that of cells that have not divided yet, as shown in Supporting Information, Figure 5). It is interesting to note that at later exposure times, when cell division is impaired, although the uptake rate seems to decrease in comparison to the first 24 h of incubation, clearly nanoparticle uptake still occurs for both EdU-positive and EdU-negative cells (Supporting Information, Figure 5). Thus, despite the cell cycle arrest, the strong perturbations of cyclin levels and the lack of DNA synthesis described, cells treated with PS-NH_2-nanoparticles did not show a strong reduction in their energy levels and continued to accumulate nanoparticles, which is also known to be an energy-dependent process.[3,9]

We also performed further numerical simulations to support our interpretation of the experimental results shown in Figure 5a. As the experimental data on cell cycle progression is qualitatively consistent with simulations of arrest at multiple points of the cell cycle, we assumed this scenario to be true in the following. In the simulations, we coupled the progression and arrest of cells along the cell cycle to a constant rate of nanoparticle uptake (as detailed in the Supporting Information and building upon our previous work).[31] As above, we investigated the effect of what fraction (0, 25, 50, and 100%) of cells that reach either checkpoint are arrested (Supporting Information, Figure 6). If none (0%) of cells are arrested, then cell division competes with nanoparticle uptake, leading to a plateau in the nanoparticle uptake kinetics, as for the case of carboxylated polystyrene shown in Figure 5a, as previously demonstrated.[31] In the other extreme, where all (100%) of the cells are arrested when they reach a checkpoint, cell division ceases rapidly and for this case, nanoparticle uptake kinetics is essentially linear for all times. Between the two extremes (0 and 100%), there is some element of cell cycle activity, though the amount of residual cell cycle activity decreases with time. Thus, the nanoparticle uptake kinetics shows some element of nonlinear behavior due to cell cycle activity (split of internalized nanoparticles upon cell division), but the linear part dominates progressively more as time goes on. The experimental results for PS-NH_2 (Figure 5a) showed qualitatively similar results (though complicating factors at late times were not taken into account in the simulations).

An idealization we used in the simulations is that we assumed that the given fraction (0, 25, 50, or 100%) of cells that were arrested when they reached a checkpoint was constant in time. Conceivably, this fraction could vary with time as nanoparticles are internalized. To investigate how sensitive the results could be to such time variations, we investigated some extreme examples of time variation, wherein we kept the fraction of arresting cells constant in time, but delayed the time at which the cell cycle arrest started. The results turned out to be rather insensitive to the timing (Supporting Information, Figure 6). Hence, we believe the idealized picture to be qualitatively correct.

The effect of the absence of cell division on the internalized nanoparticle load could also be observed when fluorescent nanoparticle-loaded cells were further grown in either nanoparticle-free medium or nonfluorescent nanoparticle-containing medium (Figure 5b). When the cell cycle progressed normally, as in the case of cells treated with PS-COOH nanoparticles (data reproduced from ref 31 are shown for comparison), a gradual decrease of the internalized nanoparticle load was observed over time as the cells divided (Figure 5b; gray). However, when after 24 h of exposure to PS-NH_2 nanoparticles, the arrested cells were further grown in nanoparticle-free medium, the initial load of internalized nanoparticles was also diluted over time, though to a lesser extent (Figure 5b; red). This is, again, consistent with not all cells having yet arrested after 24 h of treatment with PS-NH_2, but could also be interpreted as some cells being able to recuperate from the arrest. It appears as if there is significant cell cycle progression occurring after PS-NH_2 treatment and subsequent incubation in nanoparticle-free medium (Supporting Information, Figure 7). Still, these results are not conclusive as to whether cells can recuperate from the arrest or not, and to completely disentangle the two effects one would need an explicit marker for arrested cells. When instead the arrested cells were further grown in medium containing nonfluorescent PS-NH_2 nanoparticles, the intracellular concentration of the fluorescent nanoparticles remained roughly constant over time (Figure 5b; black), as a consequence of the low amount of cell division taking place due to the uninterrupted exposure to PS-NH_2 nanoparticles. This also suggested the absence of significant nanoparticle export, as has also been reported for other examples of nanoparticles accumulating in the lysosomes.[3,9,31]

Finally, nanoparticle localization was studied by fluorescence microscopy during the 72 h of exposure in order to understand the final fate of the nano particles inside the cells. Confocal images confirmed nanoparticle internalization and, consistent with what has previously been reported, immunostaining of subcellular compartments showed the final intracellular destination to (predominantly) be the lysosomes (Figure 6a).[20] After 6 h of incubation, PS-NH_2 nanoparticles were detected inside the cells and some degree of colocalization with the lysosomes (LAMP1-positive vesicles) was observed. At later stages, colocalization increased notably and, more importantly, lysosomes loaded with PS-NH_2 nanoparticles appeared enlarged. Similar observations on lysosomes have been reported for higher doses of the same nanoparticles,[20,24] although in those conditions, lysosomal swelling was accompanied by leakage of proteolytic enzymes into the cytosol and, finally, activation of cell death pathways.[24] It has been proposed that the effect of cationic nanoparticles on lysosomes could be due to a mechanism called the proton sponge in which the amine groups on the nanoparticles' surface get protonated inside the acidic organelles and increase the osmotic pressure of the vesicles due to the internalization of neutralizing ions and water.[48−50] However, data on nonprotonable cationic nanoparticles suggest that protonation alone would not be enough to account for nanoparticle-induced lysosomal damage.[23,24] To further study the observed swelling and investigate if lysosomal membrane permeability was compromised in the exposure conditions applied here, PS-NH_2-treated cells were stained with the acidotropic dye LysoTracker Red (Figure 6b). An increase in the mean intensity of the staining was found for the PS-NH_2-treated cells, which is consistent with the increase in the volume of acidic subcellular compartments observed by confocal imaging. Loss of LysoTracker staining can be observed as a second peak at much lower intensities when higher doses of PS-NH_2 nanoparticles are applied (see 72 h panel in Figure 6b), and this is a sign of compromised lysosomal membrane integrity.[24] However, at the nanoparticle concentration used here (25 μg/mL), the second peak at lower intensity was not observed for short incubation times, and given that in these conditions cell death levels were low, the results suggest that despite the observed lysosomal swelling the severity of the damage to such organelles was less than that described for higher nanoparticle doses at which cell death is induced. In agreement with this, the presence of the lysosomal protease cathepsin was not obvious in the cytosol, as opposed to what is observed at higher nanoparticle doses (Supporting Information, Figure 8).

Although a clear connection between cell cycle regulation and lysosomal function has not been reported yet, it has been shown that drugs that induce lysosomal damage, such as, for instance, chloroquine,[51] can lead to cell cycle arrest and cell death due to interference with autophagic processes,[52] and similarly some findings in other model systems have connected cathepsins and mitotic events.[53] This overall suggests that the effects observed on cell cycle progression may be connected to the lysosomal alterations detected upon exposure to the PS-NH_2 nanoparticles and accumulation in the lysosomes.

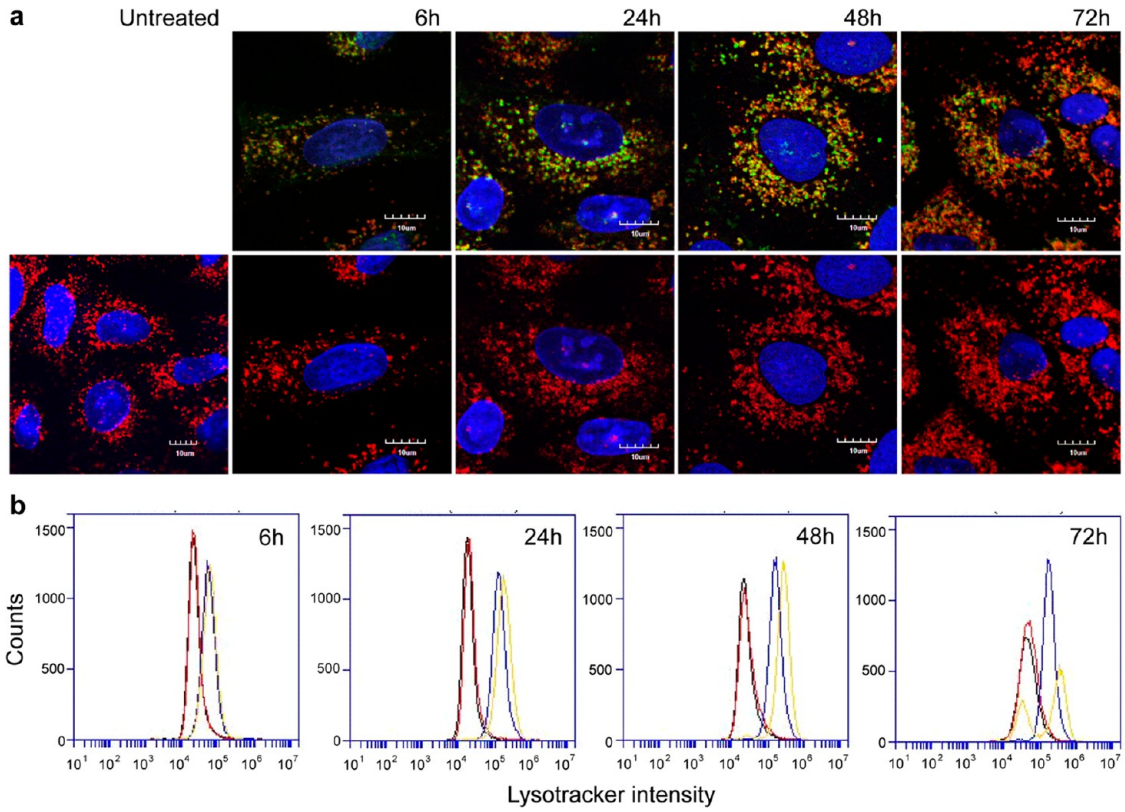

Figure 6. Amino-modified polystyrene nanoparticles accumulate in the lysosomes, causing their enlargement and compromising their membrane integrity. (a) Confocal images of cells incubated with 25 μg/mL amino-modified polystyrene (PS-NH_2) nanoparticles for 6−72 h. Different colors are applied to improve visualization: nuclei (Draq5) are shown in blue; lysosomes (LAMP1) in red; nanoparticles in green. Top images are overlapped channels for nuclei, lysosomes, and nanoparticles; bottom images show the same without the nanoparticle channel. (b) Enlargement of lysosomes due to treatment with PS-NH_2 nanoparticles. Lysotracker fluorescence intensity of cells incubated for 6, 24, 48, and 72 h with cMEM (black), carboxylated polystyrene at 25 μg/mL (red), or amino-modified polystyrene nanoparticles at 25 μg/mL (blue) or 50 μg/mL (yellow), measured by flow cytometry.

More efforts are needed in this direction in order to fully elucidate the origin of the observed cell cycle arrest.

CONCLUSIONS

In conclusion, the potential of PS-NH_2 to induce cell death at high concentrations has been extensively described.[20,23,24] At the lower concentrations studied here, PS-NH_2 accumulated in the lysosomes and lysosomal swelling was observed. Although at this dose the swelling was not accompanied by severe loss of lysosomal membrane integrity and strong cell death (as reported for higher nanoparticle doses), a different outcome was instead observed wherein cell cycle progression was impaired. Strong perturbations of cyclin levels were detected already after 6 h, together with lack of DNA synthesis and inhibition of cell proliferation. Using a combination of numerical simulations and experiments, we suggest that the observed impairment of the cell cycle is consistent with combined arrest at the transitions between G1/S and G2/M phases, and that the arrest occurs gradually. Of noteworthy, despite the cell cycle being arrested, the intracellular ATP level did not decrease and nanoparticle internalization (an energy-dependent process) did not cease either. Although further work is needed in order to elucidate the mechanism of action of PS-NH_2, the results presented here clearly show that the same nanoparticles hold the potential to activate very different cellular signals and, in this example, either induce cell cycle arrest or trigger cell death pathways depending on the intracellular load achieved.

The effects on cell cycle progression were also reflected in nanoparticle accumulation kinetics. Comparing with previous experimental results and also using numerical simulations, we demonstrated the strong connection between cell cycle progression and nanoparticle accumulation, both in the presence and absence of cell division. We previously demonstrated that, in the presence of cell division, the internalized nanoparticles are split among daughter cells when the cell divides, thereby lowering the nanoparticle dose over time. Here, on the other hand, we found that when cells do not divide, which in this case is an effect of the accumulation of the nanoparticles themselves, relatively higher accumulation levels of nanoparticles are achieved.

Finally, because lysosomal alterations were observed also in the conditions studied here, and considering that many other nanoparticles are known to accumulate in

the lysosomes, these results constitute an ulterior example of the centrality of lysosomal signaling for answering and understanding nanosafety concerns, though in some cases such as this one, a clear link with the observed effects is yet missing and needs to be elucidated.

METHODS

Cell Culture. Tissue culture reagents were purchased from GIBCO Invitrogen Corporation/Life Technologies Life Sciences (Carlsbad, CA, U.S.A.). A549 cells (ATCC−CCL-185) were maintained as monolayer cultures in MEM supplemented with 10% FBS, 1% penicillin-streptomycin, and 1% nonessential amino acids (cMEM) at 37 °C and 5% CO_2.

Nanoparticles. Fluorescently labeled amino-modified polystyrene nanoparticles (PS-NH_2, Sigma, blue, 50 nm) and carboxylate-modified (PS-COOH, Invitrogen, yellow-green, 40 nm) were used without further modification or purification. Nanoparticle size (hydrodynamic diameter) by dynamic light scattering (DLS) and zeta potential were measured using Malvern Zetasizer Nano ZS90 (Worcestershire, U.K.). Freshly prepared nanoparticle dispersions were characterized in water, phosphate buffered saline (PBS), and complete cell culture media (cMEM) at 25 °C. DLS measurements are the average of a minimum of five runs, each containing 100 submeasurements; results are reported in Supporting Information, Table S1.

Flow Cytometry Assays. The 35 mm diameter plates were seeded with 150000 cells, which were grown for 24 h. Under these conditions, the cell culture is, at the start of the experiment, asynchronous. Cells were incubated with 10 μM EdU (5-ethynyl-2′-deoxyuridine) nucleoside analogue in cMEM for 30 min at 37 °C prior to (in the experiments where cell cycle progression was monitored) or after nanoparticle exposure (where the proliferative percentage was estimated). Nanoparticle dispersions were freshly prepared under sterile conditions by diluting the stock in cMEM to the required concentration, immediately prior to their addition to plates. Cells were harvested with 0.05% Trypsin-EDTA and finally fixed and stained using the Click-iT EdU Flow Cytometry Kit (Invitrogen Corporation/Life Technologies Life Sciences, CA, U.S.A.), following manufacturer's instructions. For the staining of total DNA, the Red Cell Cycle dye (7-AAD) provided in the kit was used. Sample analysis was carried out on Dako CyAn-ADP flow cytometer equipped with 405 and 488 nm lasers. A total of 15000 events were acquired per sample. Data were analyzed using the Summit software (DAKO).

To study uptake kinetics, cells were incubated with nanoparticles for different time intervals (nanoparticle dispersions were prepared immediately prior to their addition to plates by diluting the stock in cMEM to the required concentration), harvested with 0.05% Trypsin-EDTA and fixed with 4% formaline (Sigma-Aldrich) before their resuspension in PBS and analysis by flow cytometry.

Effect on lysosomes was studied using the Lysotracker dye (Invitrogen Corporation/Life Technologies Life Sciences, Carlsbad, CA, U.S.A.). After incubation with nanoparticles, cells were harvested and incubated with 50 nM Lysotracker in cMEM for 20 min at 37 °C. Finally, cells were washed and resuspended in PBS for their analysis by flow cytometry.

Cell cycle synchronization was performed by two different means. Mitotic arrest was induced by incubating cells with 200 nM nocodazole[43] (Sigma-Aldrich) for 15 h. Mitotic cells were then shaken-off, washed with PBS, and transferred to new plates with nocodazole-free medium containing the different nanoparticles as well as EdU in order to monitor S-phase entry. Samples were fixed with 4% formaline, stained using the Click-iT EdU Flow Cytometry Kit (Invitrogen Corporation/Life Technologies Life Sciences, CA, U.S.A.), following manufacturer's instructions and finally analyzed by flow cytometry every 3 h for a period of 15 h. G1/S synchronization was achieved by double thymidine block.[44] Cells were incubated with 2.5 mM thymidine (Sigma-Aldrich) for 16 h, washed with PBS, and further incubated in thymidine-free medium for 10 h. Subsequently, cells were incubated again with thymidine for 12 h, washed with PBS, and placed in thymidine-free medium with the different nanoparticles. Samples were taken at regular intervals for a period of 24 h. After fixation with 4% formaline (Sigma-Aldrich), cells were stained with MPM2 antibody (Millipore, MA, U.S.A.) in order to evaluate their entry into mitosis and with PI staining to enable total DNA content analysis.

Cell Numbers. To monitor cell numbers during continuous exposure to nanoparticles, samples were harvested at different exposure times, resuspended in 1 mL of PBS, and counted manually with 0.4% Trypan blue (HyClone, Thermo Fisher Scientific, IL, U.S.A.) in a hemocytometer chamber. Results are expressed as percentage of the number of cells in untreated cultures at the beginning of the experiment (0 h exposure).

ATP Content Luminiscence Assay. Intracellular levels of adenosine triphosphate (ATP) were quantified with the CellTiter-Glo Luminescent Cell Viability Assay (Promega Corporation, U.S.A.) according to the manufacturer's recommendations. Relative luminescent units (RLU) were detected with Varioskan Flash plate reader (Thermo Fisher Scientific, IL, U.S.A.). Results are presented as percentages of the values obtained for untreated cells. Where the aim was to analyze cell viability, the assay was performed on 96-well plates in which 10000 cells were seeded per well. On the following day, cells were exposed to the nanoparticles for 24 h prior to ATP measurements. Where the aim was instead to measure the levels of ATP per cell after exposure to nanoparticles, the ATP content of equal cell numbers was measured for all the treatments. For this purpose, 150000 cells were seeded in 35 mm diameter plates on the day before the treatments. Thus, cells were exposed to nanoparticles, and after 24 h, cells were harvested and the cell number was determined as described above. Then, for each sample, 10000 cells per well were transferred to 96-well plates, and ATP levels were measured as described above.

Confocal Imaging. A total of 150000 A549 cells were grown on 15 mm glass coverslips inside a 35 mm plate for 24 h prior to nanoparticle exposure for different time intervals. Cells were fixed and permeabilized with ice-cold methanol for 4 min and stained with anti-LAMP1 antibody (ABcam, U.K.) and green Alexa488 antimouse secondary antibody (ABcam, U.K.). Nuclei were stained with DRAQ5 (Sigma-Aldrich Fine Chemical Co., St. Louis, MO, U.S.A.). Cells were imaged with LSM500 Zeiss confocal microscope using the lasers 364, 488, and 633 nm.

Cellular Fractionation and Immunoblot Assay. Cytosolic and membrane fractions were obtained from nanoparticle-treated cultures using a previously described protocol.[54] Briefly, nanoparticle-treated cells were harvested and incubated in MSH buffer with protease inhibitor (Roche Diagnostics, U.K.) for 45 min on ice. Cells were lysed mechanically with a syringe until 50% of the cells were trypan blue-positive and then ultracentrifuged at 100000 g for 40 min at 4 °C in a Beckman-Coulter Optima L-100XP ultracentrifuge, rotor SW 55Ti. The cytosolic fraction contained in the supernatant was separated from the membrane fraction (pellet) which was further lysed in MSH buffer with 1% Triton for 15 min on ice. After centrifugation at 10000 rcf for 10 min at 4 °C, the membrane fraction contained in the supernatant was collected. Protein quantification was performed using the BCA Protein Assay Reagent kit (Thermo Fisher Scientific, IL, U.S.A.).

For Western blot analysis, a formerly published protocol was followed.[55] Briefly, 8 μg of protein was resolved by 10% SDS-PAGE and transferred onto PVDF membranes, which were probed with anti-Cathepsin L primary antibody (Cell Signaling, MA, U.S.A.) and detected with horseradish peroxidise-conjugated antimouse secondary antibody (Sigma-Aldrich Fine Chemical Co., St. Louis, MO, U.S.A.), using the ECL chemoluminiscence kit (Thermo Fisher Scientific, IL, U.S.A.) and X-ray film. Membranes were then stripped with 0,02% Sodium Azide in TBS-Tween buffer and reprobed with anti-GAPDH primary antibody (Cell Signaling, MA, U.S.A.) as a protein loading control.

Whole Cell Lysates and Immunoblot Assay. Whole cell lysates were obtained from cells incubated with amino-modified nanoparticles for different time intervals. Cells were harvested as previously explained and lysed in RIPA buffer with protease inhibitor (Roche Diagnostics, U.K.) for 15 min in ice. Samples were then centrifuged at 14000 rpm for 10 min at 4 °C and supernatant collected. Samples were quantified as explained above and probed with mouse/rabbit anti-Cyclin D1, D3, E1, A2, and B1 primary antibodies (Cell Signaling, MA, U.S.A.) and detected with horseradish peroxidase-conjugated antimouse/rabbit secondary antibody (Cell Signaling, MA, U.S.A.). Western blot analysis and protein loading control were performed as explained above.

Conflict of Interest: The authors declare no competing financial interest.

Acknowledgment. Funding was provided by the INSPIRE Programme of the Irish Government's PRTL4, National Development Plan 2007-2013 (J.A.K. and A.S.), the Small Collaborative project NanoTransKinetics (NMP4-2010-EU-US-266737) funded by the EU Seventh Framework Programme (C.Å.), Science Foundation Ireland (SFI) under Grant No. [09/RFP/MTR2425] (C.Å.) and the Irish Research Council for Science, Engineering and Technology (C.Å.). Additionally, it was supported by SFI Grant No. [SFI/SRC/B1155], the Small Collaborative project NeuroNano funded by EU Seventh Framework Programme (NNP4-SL-2008-214547) and the ESF Research Networking Programme EpitopeMap. Dr Alfonso Blanco (Flow Cytometry Core Facilities of the UCD Conway Institute) and Prof. Jeremy Simpson (Imaging facilities at UCD's School of Biology) are acknowledged for technical support. We thank Prof. Bert Vogelstein at the Johns Hopkins University for kindly providing the HCT 116 wt and p53-ko cells.

Supporting Information Available: Physicochemical characterization of nanoparticle dispersions. Effect of treatment with amino-modified polystyrene nanoparticles on p53-null and p53-wild type HCT cells. Effect of nanoparticle treatment on progression through G1/S and G2/M checkpoints of the cell cycle. Effect of nanoparticle exposure on intracellular levels of ATP. Accumulation and dilution of intracellular nanoparticle load in presence and absence of cell division. Numerical simulations of uptake kinetics in the presence and absence of cell cycle arrest. Cell cycle dynamics in arrested cells upon removal of nanoparticle source. Assessment of leakage of lysosomal contents in the cytosol. Detailed specification of the numerical simulations of cell cycle arrest. This material is available free of charge *via* the Internet at http://pubs.acs.org.

REFERENCES AND NOTES

1. Rejman, J.; Oberle, V.; Zuhorn, I. S.; Hoekstra, D. Size-Dependent Internalization of Particles *via* the Pathways of Clathrin- and Caveolae-Mediated Endocytosis. *Biochem. J.* **2004**, *377*, 159–169.
2. Chithrani, B. D.; Ghazani, A. A.; Chan, W. C. W. Determining the Size and Shape Dependence of Gold Nanoparticle Uptake into Mammalian Cells. *Nano Lett.* **2006**, *6*, 662–668.
3. Salvati, A.; Åberg, C.; dos Santos, T.; Varela, J.; Pinto, P.; Lynch, I.; Dawson, K. A. Experimental and Theoretical Comparison of Intracellular Import of Polymeric Nanoparticles and Small Molecules: Toward Models of Uptake Kinetics. *Nanomed. Nanotechnol. Biol. Med.* **2011**, *7*, 818–26.
4. Ruoslahti, E.; Bhatia, S. N.; Sailor, M. J. Targeting of Drugs and Nanoparticles to Tumors. *J. Cell Biol.* **2010**, *188*, 759–768.
5. Ferrari, M. Cancer Nanotechnology: Opportunities and Challenges. *Nat. Rev. Cancer* **2005**, *5*, 161–171.
6. Gillies, E. R.; Fréchet, J. M. J. Dendrimers and Dendritic Polymers in Drug Delivery. *Drug Discovery Today* **2005**, *10*, 35–43.
7. Brigger, I.; Dubernet, C.; Couvreur, P. Nanoparticles in Cancer Therapy and Diagnosis. *Adv. Drug Delivery Rev.* **2002**, *54*, 631–651.
8. Farokhzad, O. C.; Langer, R. Impact of Nanotechnology on Drug Delivery. *ACS Nano* **2009**, *3*, 16–20.
9. Shapero, K.; Fenaroli, F.; Lynch, I.; Cottell, D. C.; Salvati, A.; Dawson, K. A. Time and Space Resolved Uptake Study of Silica Nanoparticles by Human Cells. *Mol. BioSyst.* **2011**, *7*, 371–378.
10. Stern, S. T.; McNeil, S. E. Nanotechnology Safety Concerns Revisited. *Toxicol. Sci.* **2008**, *101*, 4–21.
11. Nel, A.; Xia, T.; Mädler, L.; Li, N. Toxic Potential of Materials at the Nanolevel. *Science* **2006**, *311*, 622–627.
12. Oberdörster, G.; Oberdörster, E.; Oberdörster, J. Nanotoxicology: An Emerging Discipline Evolving from Studies of Ultrafine Particles. *Environ. Health Perspect.* **2005**, *113*, 823–839.
13. Boraschi, D.; Costantino, L.; Italiani, P. Interaction of Nanoparticles with Immunocompetent Cells: Nanosafety Considerations. *Nanomedicine* **2011**, *7*, 121–131.
14. Roa, W.; Zhang, X. J.; Guo, L. H.; Shaw, A.; Hu, X. Y.; Xiong, Y. P.; Gulavita, S.; Patel, S.; Sun, X. J.; Chen, J.; et al. Gold Nanoparticle Sensitize Radiotherapy of Prostate Cancer Cells by Regulation of the Cell Cycle. *Nanotechnology* **2009**, *20*, 375101.
15. Wu, J.; Sun, J.; Xue, Y. Involvement of Jnk and P53 Activation in G2/M Cell Cycle Arrest and Apoptosis Induced by Titanium Dioxide Nanoparticles in Neuron Cells. *Toxicol. Lett.* **2010**, *199*, 269–276.
16. Asharani, P.; Xinyi, N.; Hande, M. P.; Valiyaveettil, S. DNA Damage and P53-Mediated Growth Arrest in Human Cells Treated with Platinum Nanoparticles. *Nanomedicine* **2010**, *5*, 51–64.
17. Asharani, P. V.; Low Kah Mun, G.; Hande, M. P.; Valiyaveettil, S. Cytotoxicity and Genotoxicity of Silver Nanoparticles in Human Cells. *ACS Nano* **2009**, *3*, 279–290.
18. Xia, T.; Kovochich, M.; Liong, M.; Mädler, L.; Gilbert, B.; Shi, H.; Yeh, J. I.; Zink, J. I.; Nel, A. E. Comparison of the Mechanism of Toxicity of Zinc Oxide and Cerium Oxide Nanoparticles Based on Dissolution and Oxidative Stress Properties. *ACS Nano* **2008**, *2*, 2121–2134.
19. Park, E.-J.; Yi, J.; Kim, Y.; Choi, K.; Park, K. Silver Nanoparticles Induce Cytotoxicity by a Trojan-Horse Type Mechanism. *Toxicol. In Vitro* **2010**, *24*, 872–878.
20. Bexiga, M. G.; Varela, J. A.; Wang, F.; Fenaroli, F.; Salvati, A.; Lynch, I.; Simpson, J. C.; Dawson, K. A. Cationic Nanoparticles Induce Caspase 3-, 7- and 9-Mediated Cytotoxicity in a Human Astrocytoma Cell Line. *Nanotoxicology* **2011**, *5*, 557–567.
21. Sabella, S.; Brunetti, V.; Vecchio, G.; Galeone, A.; Maiorano, G.; Cingolani, R.; Pompa, P. Toxicity of Citrate-Capped AuNPs: An *In Vitro* and *In Vivo* Assessment. *J. Nanopart. Res.* **2011**, *13*, 6821–6835.
22. Deng, Z. J.; Liang, M.; Monteiro, M.; Toth, I.; Minchin, R. F. Nanoparticle-Induced Unfolding of Fibrinogen Promotes Mac-1 Receptor Activation and Inflammation. *Nat. Nanotechnol.* **2011**, *6*, 39–44.
23. Xia, T.; Kovochich, M.; Liong, M.; Zink, J. I.; Nel, A. E. Cationic Polystyrene Nanosphere Toxicity Depends on Cell-Specific Endocytic and Mitochondrial Injury Pathways. *ACS Nano* **2007**, *2*, 85–96.
24. Wang, F.; Yu, L.; Monopoli, M. P.; Sandin, P.; Mahon, E.; Salvati, A.; Dawson, K. A. The Biomolecular Corona Is Retained During Nanoparticle Uptake and Protects the Cells from the Damage Induced by Cationic Nanoparticles until Degraded in the Lysosomes. *Nanomed. Nanotechnol. Biol. Med.* **2013**, 10.1016/j.nano.2013.04.010.
25. Liu, Y.; Li, W.; Lao, F.; Liu, Y.; Wang, L.; Bai, R.; Zhao, Y.; Chen, C. Intracellular Dynamics of Cationic and Anionic Polystyrene Nanoparticles without Direct Interaction with Mitotic Spindle and Chromosomes. *Biomaterials* **2011**, *32*, 8291–8303.
26. Lunov, O.; Syrovets, T.; Loos, C.; Nienhaus, G. U.; Mailänder, V.; Landfester, K.; Rouis, M.; Simmet, T. Amino-Functionalized Polystyrene Nanoparticles Activate the NLRP3 Inflammasome in Human Macrophages. *ACS Nano* **2011**, *5*, 9648–9657.
27. Sandin, P.; Fitzpatrick, L. W.; Simpson, J. C.; Dawson, K. A. High-Speed Imaging of Rab Family Small GTPases Reveals Rare Events in Nanoparticle Trafficking in Living Cells. *ACS Nano* **2012**, *6*, 1513–1521.

28. Ma, X.; Wu, Y.; Jin, S.; Tian, Y.; Zhang, X.; Zhao, Y.; Yu, L.; Liang, X.-J. Gold Nanoparticles Induce Autophagosome Accumulation through Size-Dependent Nanoparticle Uptake and Lysosome Impairment. *ACS Nano* **2011**, *5*, 8629–8639.
29. Malumbres, M.; Barbacid, M. Cell Cycle, CDKs and Cancer: A Changing Paradigm. *Nat. Rev. Cancer* **2009**, *9*, 153–166.
30. Schwartz, G. K.; Shah, M. A. Targeting the Cell Cycle: A New Approach to Cancer Therapy. *J. Clin. Oncol.* **2005**, *23*, 9408–9421.
31. Kim, J. A.; Åberg, C.; Salvati, A.; Dawson, K. A. Role of Cell Cycle on the Cellular Uptake and Dilution of Nanoparticles in a Cell Population. *Nat. Nanotechnol.* **2012**, *7*, 62–68.
32. Röcker, C.; Pötzl, M.; Zhang, F.; Parak, W. J.; Nienhaus, G. U. A Quantitative Fluorescence Study of Protein Monolayer Formation on Colloidal Nanoparticles. *Nat. Nanotechnol.* **2009**, *4*, 577–580.
33. Lundqvist, M.; Stigler, J.; Elia, G.; Lynch, I.; Cedervall, T.; Dawson, K. A. Nanoparticle Size and Surface Properties Determine the Protein Corona with Possible Implications for Biological Impacts. *Proc. Natl. Acad. Sci. U.S.A.* **2008**, *105*, 14265–14270.
34. Monopoli, M. P.; Åberg, C.; Salvati, A.; Dawson, K. A. Biomolecular Coronas Provide the Biological Identity of Nanosized Materials. *Nat. Nanotechnol.* **2012**, *7*, 779–786.
35. Monopoli, M. P.; Walczyk, D.; Campbell, A.; Elia, G.; Lynch, I.; Baldelli Bombelli, F.; Dawson, K. A. Physical-Chemical Aspects of Protein Corona: Relevance to *In Vitro* and *In Vivo* Biological Impacts of Nanoparticles. *J. Am. Chem. Soc.* **2011**, *133*, 2525–2534.
36. van Vugt, M. A. T. M.; Yaffe, M. B. Cell Cycle Re-Entry Mechanisms after DNA Damage Checkpoints: Giving It Some Gas to Shut Off the Breaks!. *Cell Cycle* **2010**, *9*, 2097–2101.
37. Kastan, M. B.; Bartek, J. Cell-Cycle Checkpoints and Cancer. *Nature* **2004**, *432*, 316–323.
38. Vogelstein, B.; Lane, D.; Levine, A. J. Surfing the p53 Network. *Nature* **2000**, *408*, 307–310.
39. Vogelstein, B.; Kinzler, K. W. Cancer Genes and the Pathways They Control. *Nat. Med.* **2004**, *10*, 789–799.
40. Jordan, M. A.; Wilson, L. Microtubules as a Target for Anticancer Drugs. *Nat. Rev. Cancer* **2004**, *4*, 253–265.
41. Pedrali-Noy, G.; Spadari, S.; Miller-Faures, A.; Miller, A. O. A.; Kruppa, J.; Koch, G. Synchronization of HeLa Cell Cultures by Inhibition of DNA Polymerase α with Aphidicolin. *Nucleic Acids Res.* **1980**, *8*, 377–387.
42. Åberg, C.; Kim, J. A.; Salvati, A.; Dawson, K. A. Theoretical Framework for Nanoparticle Uptake and Accumulation Kinetics in Dividing Cell Populations. *Europhys. Lett.* **2013**, *101*, 38007.
43. Vasquez, R. J.; Howell, B.; Yvon, A. M. C.; Wadsworth, P.; Cassimeris, L. Nanomolar Concentrations of Nocodazole Alter Microtubule Dynamic Instability *In Vivo* and *In Vitro*. *Mol. Biol. Cell* **1997**, *8*, 973–985.
44. Harper, J. V., Synchronization of Cell Populations in G1/S and G2/M Phases of the Cell Cycle. In *Cell Cycle Control*; Humphrey, T.; Brooks, G., Eds.; Humana Press: NJ, 2005; Vol. 296, pp 157−166.
45. Davis, F. M.; Tsao, T. Y.; Fowler, S. K.; Rao, P. N. Monoclonal Antibodies to Mitotic Cells. *Proc. Natl. Acad. Sci. U.S.A.* **1983**, *80*, 2926–2930.
46. Sherr, C. J.; Roberts, J. M. Living with or without Cyclins and Cyclin-Dependent Kinases. *Genes Dev.* **2004**, *18*, 2699–2711.
47. Smits, V. A. J.; Medema, R. H. Checking out the G2/M Transition. *Biochim. Biophys. Acta, Gene Struct. Express.* **2001**, *1519*, 1–12.
48. Nel, A. E.; Mädler, L.; Velegol, D.; Xia, T.; Hoek, E. M. V.; Somasundaran, P.; Klaessig, F.; Castranova, V.; Thompson, M. Understanding Biophysicochemical Interactions at the Nano-Bio Interface. *Nat. Mater.* **2009**, *8*, 543–557.
49. Nabiev, I.; Mitchell, S.; Davies, A.; Williams, Y.; Kelleher, D.; Moore, R.; Gun'ko, Y. K.; Byrne, S.; Rakovich, Y. P.; Donegan, J. F.; et al. Nonfunctionalized Nanocrystals Can Exploit a Cell's Active Transport Machinery Delivering Them to Specific Nuclear and Cytoplasmic Compartments. *Nano Lett.* **2007**, *7*, 3452–3461.
50. Steinberg, B. E.; Huynh, K. K.; Brodovitch, A.; Jabs, S.; Stauber, T.; Jentsch, T. J.; Grinstein, S. A Cation Counterflux Supports Lysosomal Acidification. *J. Cell Biol.* **2010**, *189*, 1171–1186.
51. Jiang, P.-d.; Zhao, Y.-l.; Shi, W.; Deng, X.-q.; Xie, G.; Mao, Y.-q.; Li, Z.-g.; Zheng, Y.-z.; Yang, S.-y.; Wei, Y.-q. Cell Growth Inhibition, G2/M Cell Cycle Arrest, and Apoptosis Induced by Chloroquine in Human Breast Cancer Cell Line Bcap-37. *Cell. Physiol. Biochem.* **2008**, *22*, 431–440.
52. Yoon, Y. H.; Cho, K. S.; Hwang, J. J.; Lee, S.-J.; Choi, J. A.; Koh, J.-Y. Induction of Lysosomal Dilatation, Arrested Autophagy, and Cell Death by Chloroquine in Cultured ARPE-19 Cells. *Invest. Ophthalmol. Vis. Sci.* **2010**, *51*, 6030–6037.
53. Morin, V.; Sanchez, A.; Quiñones, K.; Huidobro, J. G.; Iribarren, C.; Bustos, P.; Puchi, M.; Geneviève, A. M.; Imschenetzky, M. Cathepsin L Inhibitor I Blocks Mitotic Chromosomes Decondensation During Cleavage Cell Cycles of Sea Urchin Embryos. *J. Cell. Physiol.* **2008**, *216*, 790–795.
54. Oberle, C.; Huai, J.; Reinheckel, T.; Tacke, M.; Rassner, M.; Ekert, P. G.; Buellesbach, J.; Borner, C. Lysosomal Membrane Permeabilization and Cathepsin Release Is a Bax/Bak-Dependent, Amplifying Event of Apoptosis in Fibroblasts and Monocytes. *Cell Death Differ.* **2010**, *17*, 1167–1178.
55. Burnette, W. N. "Western Blotting": Electrophoretic Transfer of Proteins from Sodium Dodecyl Sulfate-Polyacrylamide Gels to Unmodified Nitrocellulose and Radiographic Detection with Antibody and Radioiodinated Protein A. *Anal. Biochem.* **1981**, *112*, 195–203.